Three-phase flow simulation of local scour around a submerged horizontal cylinder

Shijie Huang[a],Zhenhua Huang[a,*]
[a] Department of Ocean and Resources Engineering, School of Ocean and Earth Science and Technology,
University of Hawaii at Manoa, Honolulu, HI, 96822, USA
[*] Corresponding author contact: zhenhua@hawaii.edu

ABSTRACT

Wave-induced scour plays a key role in the stability analysis of coastal structures, submarine pipelines or cables. There is a rich literature in current-induced scour, but more research is needed to understand the characteristics of wave-induced scour and the mechanisms that are important to the scour process. Sediment transport and flow-induced scour are three-phase (air-water-sediment) flow problems in nature and multi-phase flow simulation is a useful tools that can provide information difficult to obtain from physical tests. Most existing numerical models developed for simulating local scours are based on one-way coupling, which neglects effects of sediment phase on hydrodynamics of the flow. The present study uses a three-phase (air, water and sediment) flow model, which allows for a two-way coupling, to simulate wave-induced local scour problems. The three-phase flow model captures the air-water interface using a modified VOF method, and uses an improved rheology for the sediment phase for better results. The model is validated and verified using one set of existing experiment results for local scour around a submerged horizontal pipe. The detailed flow fields of both the sediment phase and the water phase around the scour are analyzed to understand the scour process. All three-phase flow simulations flow simulations on XSEDE's Stampede2 supercomputers. The applicability of the model to other local scour problems is also discussed.

KEY WORDS: Sediment transport; Wave-induced scour; vortex shedding.

INTRODUCTION

Sediment transport involves interaction between water/air and sediment, which is a complicated process frequently happening in nature. Understanding sediment transport is critical for some engineering projects involving pipelines or power cables on seafloor and oil platforms. The interaction between sediment and the flow around the structures may cause local morphological changes: an increased flow rate might lead to local erosion while decreased flow rate may result in deposition. The foundation stability will be affected by these processes.

Most existing numerical models treat sediment transport as a passive motion (one-way coupling) following the flow (Roulund et al., 2005) and the transport rate is calculated using published empirical formulas (Lee et al., 2019); this is due to the poor understanding of micro-scale hydrodynamics, turbulence and the computing power available at the time when these models were developed. For instance, Roulund et al. (2005) studied, both numerically and experimentally, the flow and local scour around a vertical pile exposed to a steady current and found that the scour depth was highly affected by the local flow pattern around the pile, such as horseshoe vortex and lee-wake vortex. Wu et al. (2000) developed a three-dimensional (3D) sediment transport model, which treats the bed-load and suspended-load with different empirical or semi-empirical equations, and simulated the sediment transport in an open channel flow; however, the agreement between the numerical and experimental results is less satisfactory close to the bank. Wave-induced sediment transport and scour around a pipeline is a multi-phase phase problem in nature. Even though one-way coupling models are suitable for large-scale practical problem, they do not have a direct consideration on the influence of sediment motion on the flow characteristics. The rapid development of computer hardware has made it possible to develop two-way coupled multi-phase flow models to understand physics involved in the interaction between the sediment and fluid phases and to better simulate the sediment transport and scour processes.

The work presented in this study is based on a full-way coupled, two-phase flow model developed by Lee et al. (2016) and Lee et al. (2019). The implementation of this model is through the open source CFD toolbox OpenFOAM OpenCFD. This model has been used to study the local scour under a pipeline exposed to steady current and local scour caused by a submerged jet flow. This study attempts to use this three-phase flow model to study the local scour around a submerged horizontal pipeline exposed to regular waves, which was experimentally studied by Sumer and Fredsøe (1990). The simulated flow fields of both the fluid phase and the sediment phase around the pipeline and development of the scour depth underneath the pipe will be presented.

Limitations of the present study and possible improvement in the future are also discussed.

GOVERNING EQUATIONS

The mathematical formulation of the three-phase flow model is summarized here for completeness. A volume-of fluid (VOF) method proposed by Hirt and Nichols (1981) is employed to track the air-water free surface. The VOF method defines a liquid saturation s, which represents the volume fraction of water in a certain control volume. $s = 0$ means the control volume is occupied by air only and $s = 1$ means the control volume is occupied by water only. Instead of a sharp transition from pure water to pure air, the free surface is modeled by a narrow region where the liquid saturation s is between 0 and 1. Due to the diffusive nature of this narrow layer (VOF layer) where the fluid is a mixture of the air and water, the numerical free surface is defined by specifying an appropriate value for s, say 0.5. The air-water mixture can be treated as a single phase with its variable density ρ_f and dynamic viscosity ν_f determined by:

$$\rho_f = s\rho_w + (1-s)\rho_a \tag{1}$$

$$\nu_f = s\nu_w + (1-s)\nu_a \tag{2}$$

where the subscripts w and a denote water and air respectively.

In the VOF layer, there may exist suspended sediment. The volume fraction of sediment is denoted by c. The continuity equation for the sediment phase is (Christopher, 2005; Lee et al., 2019):

$$\frac{\partial c}{\partial t} + \nabla\cdot[c\mathbf{u}^s] = 0 \tag{3}$$

where $\mathbf{u}^s$ is the velocity of the sediment phase; The continuity equation for the water phase is

$$\frac{\partial(1-c)s}{\partial t} + \nabla\cdot[(1-c)s\mathbf{u}^f] = 0 \tag{4}$$

where $\mathbf{u}^f$ is the velocity of the fluid phase. Consequently, the continuity equation for the gaseous phase is

$$\frac{\partial(1-c)(1-s)}{\partial t} + \nabla\cdot[(1-c)(1-s)\mathbf{u}^f] = 0 \tag{5}$$

Below the air-water interface, there are water phase and sediment phase. The sediment is assumed to be absent above VOF layer and thus the momentum equations for the fluid and sediment phases are (Lee et al., 2019):

$$\begin{aligned}\frac{\rho_s c\mathbf{u}^s}{\partial t} + \nabla\cdot[\rho_s c\mathbf{u}^s\mathbf{u}^s] &= \rho_s cg - c\nabla p_f - \nabla(cp_s) + \nabla\cdot[c\mathbf{T}^s]\\ &+c\rho_s\frac{\mathbf{u}^f-\mathbf{u}^s}{\tau_p} - \frac{\rho_s}{\tau_p}\frac{(1-c)\nu_{ft}}{\sigma_c}\nabla c\end{aligned} \tag{6}$$

for the sediment phase, and

$$\begin{aligned}\frac{\rho_f(1-c)\mathbf{u}^f}{\partial t} + \nabla\cdot[\rho_f(1-c)\mathbf{u}^f\mathbf{u}^f] &= \rho_f(1-c)g - (1-c)\nabla p_f\\ +\nabla\cdot[(1-c)\mathbf{T}^f] - c\rho_s\frac{\mathbf{u}^f-\mathbf{u}^s}{\tau_p} &+ \frac{\rho_s}{\tau_p}\frac{(1-c)\nu_{ft}}{\sigma_c}\nabla c\end{aligned} \tag{7}$$

for the fluid phase. In Eqs. 6 and 7, the subscripts or superscripts s and f stand for sediment and fluid phase, respectively. $\mathbf{u}$ is velocity, $\mathbf{g}$ gravitational acceleration, p pressure, $\mathbf{T}$ stress tensor, ν_{ft} eddy viscosity of the fluid phase and σ_c the Schmidt number. The particle response time τ_p is computed by following equation (Engelund, 1953):

$$\tau_p = \frac{\rho_s d^2}{\rho_{ff}}\frac{1}{a_E c^2 + b_E Re_p} \tag{8}$$

where a_E and b_E are model parameters with a value of 15000 and 3.6, respectively. In the momentum equations, the second last term account for the momentum exchange between sediment and fluid due to drag force and the last term account for momentum exchange due to turbulent dispersion.

A $k-\epsilon$ turbulence model similar to that in Lee et al. (2016) is adopted to calculate $\mathbf{T}^f$. The turbulence kinetic energy k and its dissipation rate ϵ are calculated with the following equations:

$$\begin{aligned}&\frac{\partial\rho_f(1-c)k}{\partial t} + \nabla\cdot[\rho_f(1-c)\mathbf{u}^f k]\\ &= (1-c)\mathbf{T}^f:\nabla\mathbf{u}^f - \rho_f(1-c)\epsilon + \nabla\cdot[\rho_f\frac{\nu_{ft}}{\sigma_k}(1-c)k]\\ &-\{(\rho_s-\rho_f)\frac{(1-c)\nu_{ft}}{\sigma_c}\nabla c\cdot\mathbf{g} + \frac{2\rho_s c(1-\alpha)k}{\tau_p}\}\end{aligned} \tag{9}$$

and

$$\begin{aligned}&\frac{\partial\rho_f(1-c)\epsilon}{\partial t} + \nabla[\rho_f(1-c)\mathbf{u}^f\epsilon]\\ &= \frac{\epsilon}{k}[C_{\epsilon1}f_1(1-c)\mathbf{T}^f:\nabla\mathbf{u}^f - C_{\epsilon2}f_2\rho_f(1-c)\epsilon]\\ &+\nabla\cdot[\rho_f\frac{\nu_{ft}}{\sigma_\epsilon}(1-c)\epsilon]\\ &-\frac{\epsilon}{k}C_{\epsilon3}\{(\rho_s-\rho_f)\frac{(1-c)\nu_{ft}}{\sigma_c}\nabla c\cdot\mathbf{g} + \frac{2\rho_s c(1-\alpha)k}{\tau_p}\}\end{aligned} \tag{10}$$

where $C_{\epsilon1}$, $C_{\epsilon2}$, σ_ϵ, σ_k and f_2 are model parameters. Refer to Lee et al. (2016) for more details about the turbulence model.

NUMERICAL SETUP

Sumer and Fredsøe (1990) studied the local scour around a horizontal pipeline exposed to regular waves experimentally, and found that the scour depth beneath the pipeline was governed by the Keulegan-Carpenter (KC) number defined as:

$$KC = \frac{U_m T}{D} = \frac{2\pi a}{D} \tag{11}$$

where U_m is the maximum particle velocity outside the boundary layer, T is the wave period, a is the amplitude of the maximum particle excursion in horizontal direction, and D the pipeline diameter. The test conditions for the case 3^a in Sumer and Fredsøe (1990) are: wave height $H = 0.15$ m and wave period $T = 1.43$ s, water depth $h = 0.4$ m, pipeline diameter $D = 0.05$ m and sand size $d_{50} = 0.58$ mm. The KC number corresponding to case 3^a is 7.0. The wave length for this test is $L = 2.46$ m.

A numerical wave flume shown in Fig. 1 is used to conduct the numerical simulation. Velocities are monitored at two locations: Point 1 (blue) and Point 2 (red) as shown in Fig. 1 with blue circle and red dot respectively. The velocities at these two points will be shown later in Fig. 6.

The total length of the numerical wave flume is $8L$, with the first 2 and last 2 wavelengths used as relaxation zones for wave generation

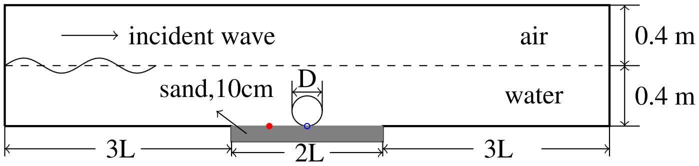

Fig. 1 A sketch of the numerical wave flume, not drawn to scale. The velocity are monitored at two locations marked by the blue circle and red dot.

and absorption, respectively. In the middle of the numerical flume is a sand pit of length $2L$ and thickness of 10 cm. It is remarked that the thickness of the sand pit in the experiment of Sumer and Fredsøe (1990) was 13 cm. Because the measured equilibrium scour depth is only about 1 cm, we believe a 3-cm difference in thickness should not affect the scour process in any significant way. The use of a slightly thinner pit can effectively reduce the number of mesh count because the grid size in this region is 2 times of the sand grain size. Because the measured scour-hole length extends only about 20 cm away from the pipeline on both sides, the length of the numerical sand pit is believed to long enough to remove any side effects. In the vertical direction, the overall height of the flume is 0.9 m, with still water surface being 0.4 m above the initial surface of the sand pit, which is at the same elevation as the false bottoms on the two sides. The pipe is fixed in this study, with its bottom just above the initial surface of the sand pit.

To save on computational resources, a set of nested grids are employed in this study. The background mesh has a size of 2 cm × 2 cm (horizontal × vertical, same for later). Close to the air-water interface (0.15 m above and below the still water surface), the mesh is refined to 2 cm × 1 cm. Close to the water-sediment interface, the mesh is refined to 0.5 cm × 0.5 cm. To better capture the scour process, the mesh size is refined to be around $2d_{50} \times 2d_{50}$ (d_{50} is the diameter of the sand) in a local region close to the pipe (0.3 m on each side of the pipe) where local scour is expected. Fig. 2 shows the over-all mesh configuration (top panel) as well as the details around the pipe (bottom panel). The total mesh count is around 0.25 million.

An example of the simulated second-order Stokes waves in an empty tank is shown in Fig. 3. The wave tank configuration and mesh distribution is done using the mesh shown in Fig. 2 except that the pipe and the inner-most mesh is removed from the flume. Virtual wave gauges are installed at three locations: one in the wave generation zone, one in the test zone and one in the wave absorption zone. As shown in Fig. 3, the wave height at the test zone is consistent with that in the wave generation zone, implying that the mesh size is fine enough to minimize the numerical attenuation during propagation. The water surface at the wave absorption zone is visually still, indicating the wave flume is free of possible reflected waves. The theoretical curve of the 2nd-order Stokes waves are also shown in Fig. 3 in the dark thick line. The slight difference between theoretical curve and test zone curve may come from the bathymetry change on the bottom.The simulated 2nd-order Stokes waves are acceptable and the mesh is suitable for the present problem.

RESULTS

Sumer and Fredsøe (1990) reported the scour profile at different instants for case 3[a]. The one at t = 12 s was compared to our numerical result in Fig. 4. It can be seen that the overall agreement is acceptable in terms of the scour depth with the present model parameters and numerical setup. However, the two deposition zones on the two sides of the pipe

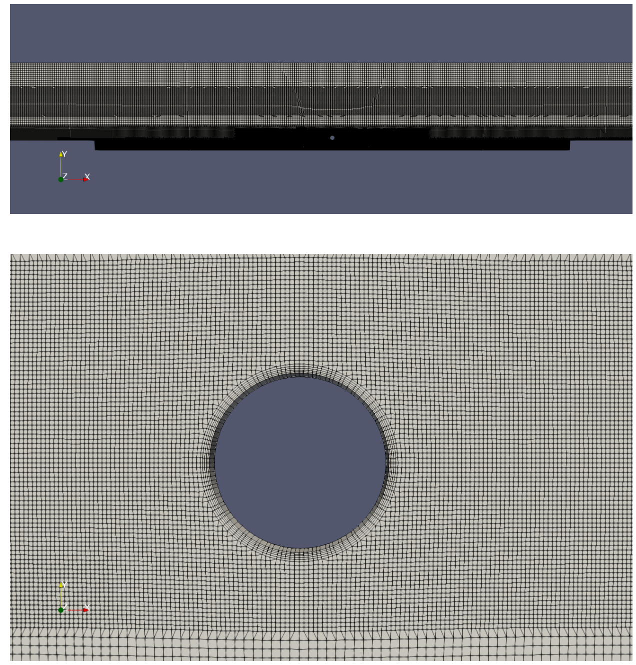

Fig. 2 Top panel show the overall mesh configuration and the bottom panel shows the inner-most mesh around the pipe and the scour region.

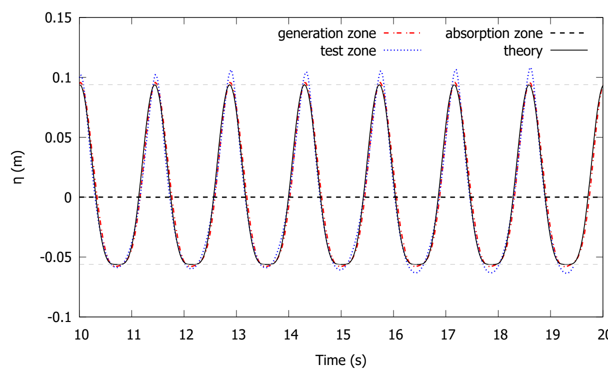

Fig. 3 Surface elevation time history at wave generation zone, test zone, and wave absorption zone, compared with theoretical curve.

are not well captured. Several factors may have contributed to this: (1) the possible difference in the initial conditions between the experiment and the numerical simulation; (2) optimization of the model parameters; (3) the definition of the sediment-fluid interface. For instance, the initial bed in the experiment might not be perfect flat while the numerical simulation has a perfectly flat initial bed. Besides, Sumer and Fredsøe (1990) only mentioned that the scour profile in Fig. 4 was taken at t = 12 s without mentioning when they started to count the time. Here the numerical scour profile is taken at 12 s after the wave generator is turned on. In the numerical simulation, the contour line of c = 0.5 is used to define the interface while in the experiment the sediment-water interface was determined visually. Furthermore, it is not clear whether or not the scour hole profile was measured by stopping the wave generator or keeping the generator running.

Fig. 5 shows the development of the scour depth beneath the pipe

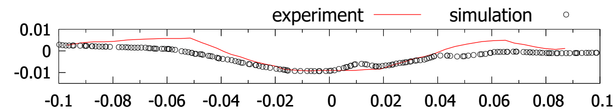

Fig. 4 Comparison of experimental and simulated sediment-water interface in the vicinity of the pipe. The pipe is not shown in the figure.

during the scour process. Scour depth is defined as the distance between the instantaneous sediment-water interface and the bottom edge of the pipe. A value of $c = 0.5$ is used to define the sediment-water interface. The scour process can be divided into two stages: onset process and scour process. Physically, the onset process has to do with the so-called piping process (see details in Discussion section). Due to the inclusion of a thin diffusion layer next to the sediment-water interface in the initial concentration to avoid numerical instability caused by a large gradient in concentration (∇c) in the governing equations, the onset process is not simulated in this study. It is believed that this numerical treatment of the initial concentration field does not have significant influence on the scour scour process.

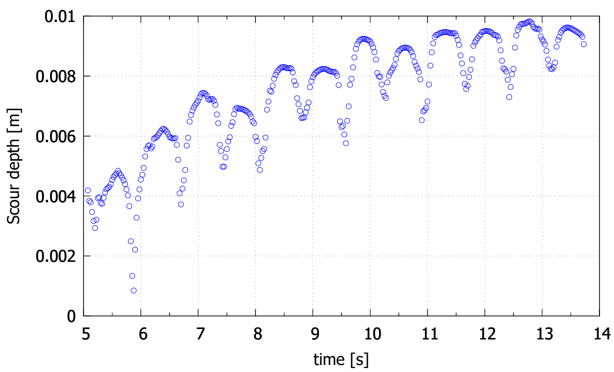

Fig. 5 Time history of scour depth beneath the pipeline

After the piping process is finished and a void is formed between the pipe and the sand below, water can pass through this void with less resistance for the water particles compared to that in the sand layer, resulting in a jet flow beneath the pipe that can carry the sand with it and transport a large amount of sand away from the pipe. As shown in Fig. 5, the scour depth is increasing faster between 6-10 s as it fluctuates twice within each wave period. Take the time period of 8.1-9.5 s as an example. During the time interval of 8.1-8.45 s, the flow beneath the pipe is moving downstream with a large amount of sediment, resulting in an increased scour depth. During the the time interval of 8.45-8.8 s, the flow is still moving downstream but with a decreased rate; this is because the sand sheet flow with $c \geq 0.5$ is passing the bottom of the pipe, resulting in a decrease in the scour depth. After that, the direction of the flow is reversed. The second peak of the scour depth at $t = 9.25$ s is lower than the previous one at $t = 8.45$ s, implying a net increase of the scour depth beneath the pipe within this period. As the scour depth increases, the flow velocity beneath the pipe slows down, resulting in a reduced scour rate. Similar processes keep on going until the scour depth reaches an equilibrium. Even at the equilibrium stage, the scour depth still fluctuates because of the sheet flow underneath the pipe. It can be concluded from Fig. 5 that the scour process is already close to the equilibrium at $t = 14$ s.

Fig. 6 shows the time history of the velocity magnitude at two different locations on the "sea floor": Point 1 is 2 mm beneath the bottom of the pipe, as denoted in Fig. 1 with blue circle. And Point 2 is $0.5L$ away from point 1 to the left, as shown in Fig. 1 with red dot. The velocity at Point 1 is the velocity of the wave-induced jet flow, which is several times stronger than the flow at Point 2.

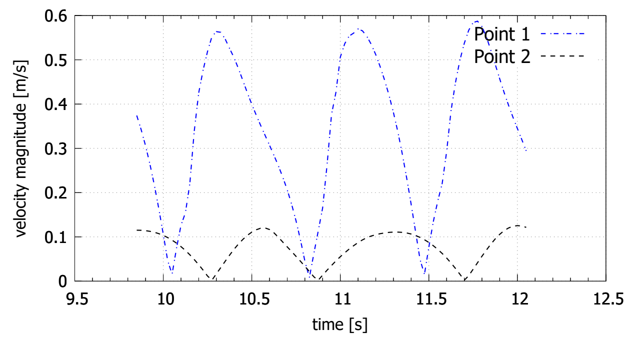

Fig. 6 Velocity magnitudes at two locations close to the pipe

Fig. 7 shows eight snapshots of the velocity field of the fluid phase in the vicinity of the pipe within the time interval of 8.1 and 9.5 s. The first 4 snapshots (a, b,c and d) correspond to the stage where the free surface is higher than the still water level while the last 4 snapshots (e, f, g and h) correspond to the stage where the free surface is lower than the still water level, as shown in the top panel. The sediment-fluid interface is determined by using $c = 0.5$. Similarly, Fig. 8 show the velocity field of the sediment phase. When the sediment concentration is lower than $c = 0.005$, the region is viewed as pure water.

According to Fig. 7, there are two main factors that dominate the scour process: the fast jet flow beneath the pipe and vortex shed from the pipe. While the former factor converts the bed-load into suspended-load and moves the bed-load, the latter controls how the suspended load is transported as the wave propagates. It can be seen that the velocity beneath the pipeline is much larger than that in other regions such as the $\pm 45^\circ$ region. Not only does this fast velocity stirs up the bed-load into suspended-load, but also it carries some bed-load with it (phase a and b). After suspension of the sand, a vortex is formed right after the pipe (phase c and d) at around the location defined by (0.02,0.01), bringing the jet-flow-induced suspended load away from the pipe. The vortex goes all the way to 0.04 m above the initial sand surface at phase d. Similar process can be found during phases e-h but when the flow reverses its direction, but with a lower strength due to the flatter trough associated with the high order Stokes wave. This will account for the asymmetry of the scour profile shown in Fig. 4. It is also worth noticing that the location where the lee-wake vortex is formed is very close to the location of the ripples shown in the experimental results but absent from the numerical simulation in Fig. 4. We suspect this is related to the turbulence model used here.

Fig. 8 shows the velocity fields of sediment phase at regions where the sediment concentration is greater than $c = 0.005$. The eight instants are consistent with those in Fig. 8. Both bed-load and suspended-load transport are included in the velocity fields by setting the cut-out concentration as $c = 0.005$. As shown in Fig. 8, the velocity magnitude at the sand-fluid interface is much greater, due to the presence of the jet flow as well as the lower concentration of sediment phase (thus density) above the interface. The jet flow carries the sand all the way to $x = 0.05$ m at phase b, and then brings part of them back at phases c and d. After

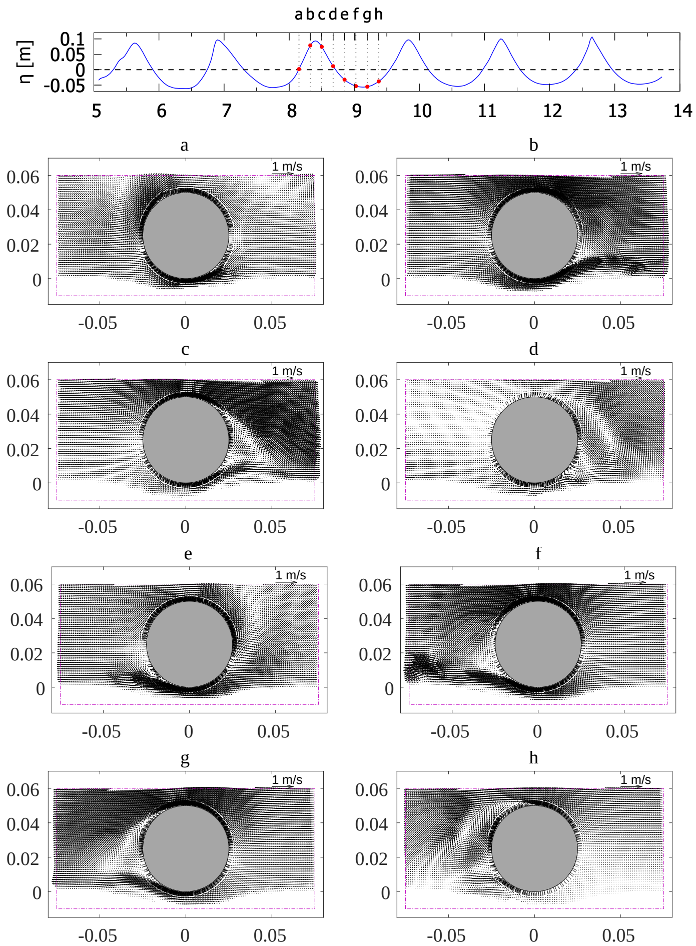

Fig. 7 Representative flow field of fluid phase after piping within one wave period. The cut-out concentration of sediment phase is $c = 0.5$

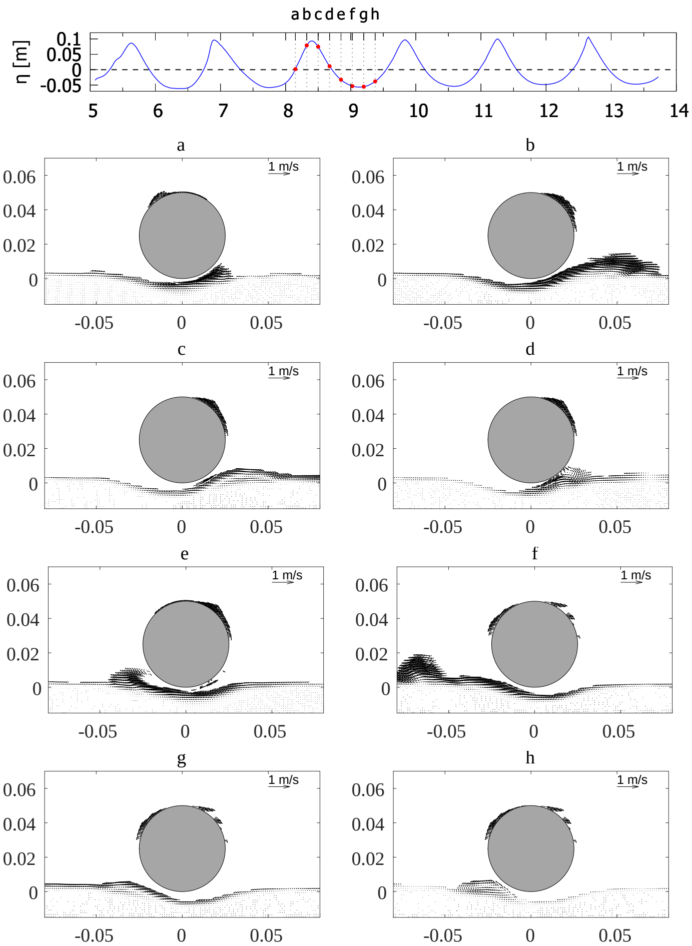

Fig. 8 Representative flow field of sediment phase after piping within one wave period. The cut-out concentration of sediment phase is $c = 0.005$

phase c, a ripple does form around (0.03, 0.005), which is very close to the final ripple location in the experimental result. However, the vortex formed at phase d, eliminates this ripple. Similar for the reverse stage during phases g and h. A ripple can be formed at (-0.03, 0.005) at phase g but the vortex eliminates it again at phase h. This suggests that the inability to capture the sand dunes on the two side as shown in Fig. 4 is related to the turbulence model used here.

DISCUSSION

The inability to simulate the onset piping process is one of the shortcomings of the present three-phase flow model. The onset process starts as the wave front reaches the pipeline and introduces a velocity field to the vicinity of the pipe. Due to the obstruction of the pipe, a pressure gradient is formed between the upstream and downstream of the pipe, driving a seepage flow beneath it. As the wave propagates, the pressure gradient may increase to a point where the induced seepage is so strong that the internal shear stress among sand particles can be destroyed. As a result, some sand beneath the pipe is carried to downstream by the seepage flow and leaving a void between the pipe and the sand below. This process is referred to as piping in soil mechanics (Terzaghi, 2007). The criterion for the piping process to occur is Terzaghi (2007):

$$\frac{\partial p}{\partial x} \leq \gamma(s-1)(1-n), \quad (12)$$

where $\partial p/\partial x$ represents the pressure gradient that drives the seepage flow beneath the pipe and γ is the specific weight of water, s is the specific gravity of sand grains defined by $s = \gamma_s/\gamma$ with γ_s being the specific weight of sand, and n is the porosity.

For the scour around a pipe exposed to regular waves, the wave-induced jet flow between the pipe and the sand-fluid interface as well as the vortexes shed from the pipe on both sides of the pipe play a key role in controlling the scour hole pattern. For the wave-induced jet flow, the momentum exchange between sand and fluid phase is a key factor determining the accuracy of the model. Our numerical experiments have shown that the results are very sensitive to the model for particle response time τ_p in Eqn. 8 because τ_P determines the drag force between the fluid phase and sediment phase. The model parameters a_E and b_E are not well understood either. A sensitivity analysis should be done in the future. For the vortex shed from the pipe, it may also contribute to the disagreement between experimental and numerical scour profile. Different turbulence models should be tested to improve the comparison with the experiment.

CONCLUSIONS

A full-way coupled, three-phase flow model was employed to simulate the scour process around a pipeline exposed to regular waves. The result shows a fairly good agreement with experimental result in terms of scour hole depth. The flow fields of both the fluid and sediment phase were analyzed by taking a representative period and it was found that the jet flow beneath the pipeline and the vortex shed from the pipe dominate the scour pattern. The agreement between the simulation and experiment can be further improved by optimizing the model parameter, which is under way and will be reported separately.

ACKNOWLEDGMENTS

This work was partially supported by the US National Science Foundation under grant No. CBET-1706938. Extreme Science and Engineering Discovery Environment (XSEDE) is also acknowledged for providing computing resources through two grants (OCE170015 and ENG180008). Any opinions, findings, and conclusions or recommendations expressed in this material are those of the author(s) and do not necessarily reflect the views of the National Science Foundation.

REFERENCES

Christopher, E.B., 2005. Fundamentals of multiphase flows. Cambridge University, Press UK .

Engelund, F., 1953. On the laminar and turbulent flows of ground water through homogeneous sand. Akad. for de Tekniske Videnskaber.

Hirt, C.W., Nichols, B.D., 1981. Volume of fluid (vof) method for the dynamics of free boundaries. Journal of computational physics 39, 201–225.

Lee, C.H., Low, Y.M., Chiew, Y.M., 2016. Multi-dimensional rheology-based two-phase model for sediment transport and applications to sheet flow and pipeline scour. Physics of Fluids 28, 053305.

Lee, C.H., Xu, C., Huang, Z., 2019. A three-phase flow simulation of local scour caused by a submerged wall jet with a water-air interface. Advances in Water Resources 129, 373–384.

OpenCFD, . The open source cfd toolbox: Programmer's guide. URL: `https://openfoam.org/`.

Roulund, A., Sumer, B., Fredsoe, J., MICHELSEN , J., 2005. Numerical and experimental investigation of flow and scour around a circular pile. Journal of Fluid Mechanics 534, 351 – 401.

Sumer, B.M., Fredsøe, J., 1990. Scour below pipelines in waves. Journal of waterway, port, coastal, and ocean engineering 116, 307–323.

Terzaghi, K., 2007. Theoretical Soil Mechanics. pp. i – xvii.

Wu, W., Rodi, W., Wenka, T., 2000. 3d numerical modeling of flow and sediment transport in open channels. Journal of hydraulic engineering 126, 4–15.